ARTICLE

Dynein activator Hook1 is required for trafficking of BDNF-signaling endosomes in neurons

Mara A. Olenick[2,3,4] , Roberto Dominguez[1,2,3], and Erika L.F. Holzbaur[1,2,3]

Axonal transport is required for neuronal development and survival. Transport from the axon to the soma is driven by the molecular motor cytoplasmic dynein, yet it remains unclear how dynein is spatially and temporally regulated. We find that the dynein effector Hook1 mediates transport of TrkB–BDNF-signaling endosomes in primary hippocampal neurons. Hook1 comigrates with a subpopulation of Rab5 endosomes positive for TrkB and BDNF, which exhibit processive retrograde motility with faster velocities than the overall Rab5 population. Knockdown of Hook1 significantly reduced the motility of BDNF-signaling endosomes without affecting the motility of other organelles. In microfluidic chambers, Hook1 depletion resulted in a significant decrease in the flux and processivity of BDNF-Qdots along the mid-axon, an effect specific for Hook1 but not Hook3. Hook1 depletion inhibited BDNF trafficking to the soma and blocked downstream BDNF- and TrkB-dependent signaling to the nucleus. Together, these studies support a model in which differential association with cargo-specific effectors efficiently regulates dynein in neurons.

Introduction

Axonal transport is vital for the maintenance and survival of neurons. Axons have a uniformly polarized microtubule array in which the faster-growing plus ends of microtubules are oriented toward the distal terminal. These microtubules serve as a highway for fast organelle trafficking mediated by molecular motors. While multiple plus end–directed kinesins are responsible for delivery of cargo to the distal end of the axon, the minus end–directed motor cytoplasmic dynein is solely responsible for trafficking a wide variety of cargo back to the soma including autophagosomes, endosomes, and mitochondria (Maday et al., 2014). These organelles not only differ in their lipid and protein compositions, but they also display distinct motility properties. It remains unclear how cytoplasmic dynein attaches to each of its cargos and how the motor is regulated to facilitate the precise trafficking of organelles to the soma.

Cytoplasmic dynein 1 (referred to in this study as dynein) is a 1.4-MD AAA$^+$ motor complex that drives the majority of minus end–directed motility in the cell. Alone, dynein is a flexible dimer with low processivity, taking many sideways or backward steps along the microtubule lattice (Reck-Peterson et al., 2006; Ross et al., 2006). Processive motility is enhanced when dynein binds to dynactin, a 1-MD multisubunit complex that reorients the dynein dimer for proper recruitment and motility along microtubules (Ayloo et al., 2014; Zhang et al., 2017). While

dynactin has been suggested to play a role in cargo interaction (Zhang et al., 2011; Yeh et al., 2012), adaptor and scaffolding proteins are required to link cargo to the dynein–dynactin motor complex (Kardon and Vale, 2009; Fu and Holzbaur, 2014). Recently, a set of coiled coil effector proteins including BICD2, Hook1, Hook3, Spindly, and NINL have been shown to enhance the dynein–dynactin interaction and induce superprocessive motility (McKenney et al., 2014; Schlager et al., 2014; Olenick et al., 2016; Schroeder and Vale, 2016; Redwine et al., 2017). BICD2, the best characterized of these dynein effectors, has been shown to increase the affinity of dynein–dynactin interaction through coiled-coil contacts along the Arp1 filament that forms the core of dynactin (Chowdhury et al., 2015; Urnavicius et al., 2015). BICD2 also interacts with the N-terminal tail of the dynein heavy chain (Chowdhury et al., 2015; Urnavicius et al., 2015) and the dynein light intermediate chain 1 (LIC1; Schroeder et al., 2014; Lee et al., 2018), leading to a stabilization of the dynein–dynactin-effector complex. Some dynein effectors can recruit two dynein dimers to a single dynactin, which further enhances the force and velocity of the motor complex (Grotjahn et al., 2018; Urnavicius et al., 2018).

Hook proteins (HookA or Hok1) are dynein effectors first characterized in filamentous fungi and shown to link dynein to early endosomes (Bielska et al., 2014; Zhang et al., 2014). In

[1]Department of Physiology, Perelman School of Medicine, University of Pennsylvania, Philadelphia, PA;   [2]The Pennsylvania Muscle Institute, Perelman School of Medicine, University of Pennsylvania, Philadelphia, PA;   [3]Biochemistry and Molecular Biophysics Graduate Group, Perelman School of Medicine, University of Pennsylvania, Philadelphia, PA;   [4]Center for Engineering Mechanobiology, University of Pennsylvania, Philadelphia, PA.

Correspondence to Erika L.F. Holzbaur: holzbaur@pennmedicine.upenn.edu.

mammalian cells, three highly conserved Hook proteins are expressed: Hook1, Hook2, and Hook3. These proteins are characterized by an N-terminal Hook domain, which binds LIC1 of dynein (Schroeder and Vale, 2016; Lee et al., 2018). The Hook domain is followed by a central coiled-coil region and a less well-conserved C-terminal cargo-binding domain (Bielska et al., 2014; Zhang et al., 2014). In vitro studies show that the binding of either Hook1 or Hook3 enhances the dynein–dynactin interaction, leading to significant increases in velocity and run lengths (McKenney et al., 2014; Olenick et al., 2016; Schroeder and Vale, 2016).

While Hook1 and Hook3 have been identified as dynein activators in vitro, the role of these proteins in dynein-mediated cargo transport in mammalian cells is less clear. Hook2 has been linked to centrosomal function and homeostasis (Szebenyi et al., 2007; Guthrie et al., 2009; Moynihan et al., 2009), while Hook1 and Hook3 have been implicated in a variety of endosomal trafficking pathways, although there is still no clear consensus on the specific roles of each isoform (Luiro et al., 2004; Xu et al., 2008; Maldonado-Báez et al., 2013). The highly polarized nature and spatial compartmentalization of neurons provide an excellent system to study the role of Hook proteins in endosomal transport. Initial work from Guo et al. (2016) suggested that Hook1 and Hook3 colocalize with retrograde Rab5a vesicles in hippocampal neurons and that knockdown (KD) of Hook1 and Hook3 reduced the retrieval of transferrin receptor from the axon (Guo et al., 2016). These data support a potential role for Hook proteins in dynein-mediated trafficking in axons, prompting us to investigate this question in more detail.

In this study, we investigated the role of Hook1 in the dynein-driven transport of endosomes along the axons of hippocampal neurons. We found that Hook1 comigrates with subpopulations of Rab5- and Rab7-positive endosomes. While loss of Hook1 did not significantly change the overall motility of Rab5- or Rab7-positive endosomes, Hook1 siRNA depletion significantly reduced the motility of a specific endosomal compartment that we identified as TrkB–brain-derived neurotrophic factor (BDNF)-signaling endosomes. The motility of TrkB–BDNF-signaling endosomes is also lost if the interaction of Hook1 with dynein is disrupted by targeted mutations at the Hook1-LIC1 interface. In addition, Hook1 is enriched in the distal axon, distinct from the cellular distribution of other dynein effectors like Rab-interacting lysosomal protein (RILP) or BICD2, suggesting a specific function in trafficking from the distal axon. Using microfluidic chambers to model the distal axonal transport of BDNF-signaling endosomes, we found that KD of Hook1 significantly reduced the flux and the processivity of BDNF transport from the distal axon to the soma. In contrast, KD of Hook3 did not affect BDNF uptake or transport. Loss of Hook1 also produced a functional block in downstream BDNF-dependent signaling to the nucleus, which is vital for neuronal survival and maintenance. Overall, this work supports a model in which Hook1 acts as a specific dynein effector for BDNF-signaling endosomes trafficking from the distal axon to induce downstream signaling in the soma of primary hippocampal neurons.
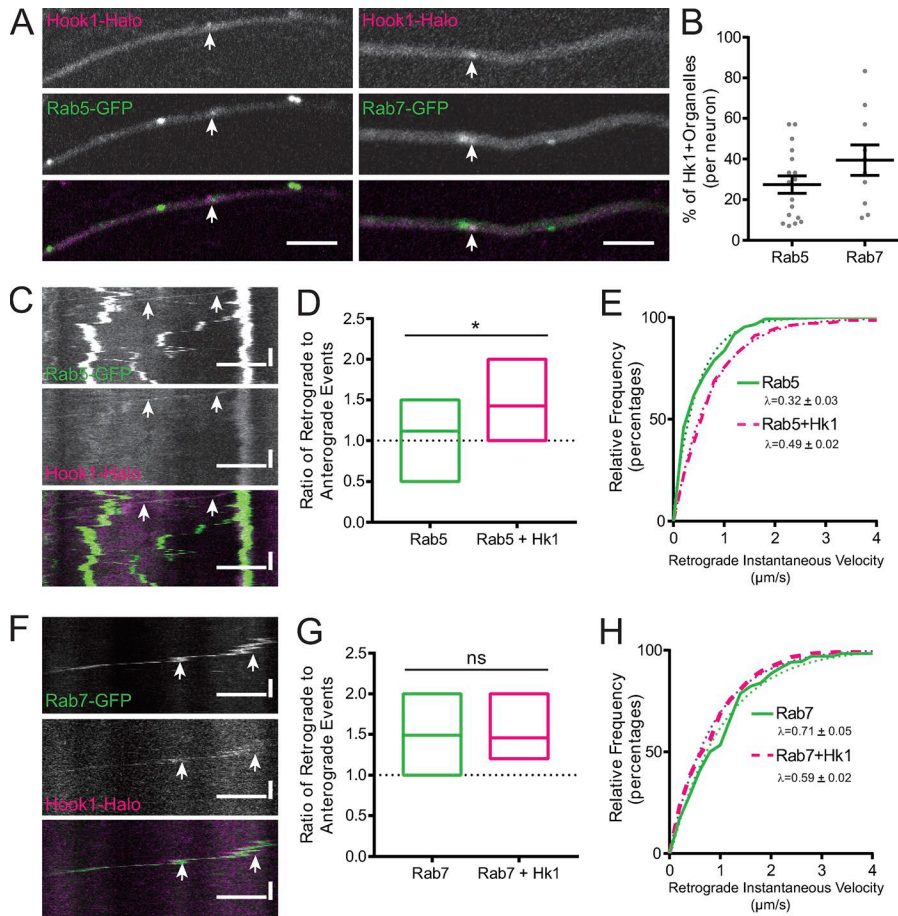
Results

Hook1 comigrates with the endosomal markers Rab5 and Rab7

To investigate the role of Hook1 in endosomal trafficking, we first expressed the early endosome marker Rab5-GFP or the late endosome marker Rab7-GFP in primary rat hippocampal neurons to observe endosomal motility. Neurons were imaged 7–8 d in vitro (DIV) at 48 h after transfection using live-cell confocal microscopy. Focusing on the axon, Rab5-GFP endosomes were found to be enriched in the distal axon, while Rab7-GFP endosomes were found throughout the distal and mid-axon. In the axon, Rab5-GFP endosomes were mainly stationary or bidirectional, with ∼80% moving <10 µm in any net direction (Fig. S1 B). In contrast, 50% of Rab7-GFP endosomes displayed net retrograde motility (Fig. S1 E).

Next, Hook1-Halo was coexpressed with Rab5-GFP or Rab7-GFP to assess whether Hook1 comigrates with a specific population of endosomes since previous studies had found Hook proteins on Rab5-positive endosomes (Bielska et al., 2014; Zhang et al., 2014; Guo et al., 2016). Surprisingly, we observed comigration of Hook1 with both a subpopulation of Rab5 endosomes and a subpopulation of Rab7 endosomes (Fig. 1, A and B). Previous in vitro research indicates that Hook1 enhances the processivity of dynein (Olenick et al., 2016), so we asked whether Hook1-positive endosomes displayed a distinctive retrograde bias in their motility or were significantly more processive than the overall population of axonal endosomes. We found that Hook1-positive Rab5 endosomes had an increased retrograde bias as seen by an increased retrograde:anterograde ratio as compared with neurons expressing Rab5-GFP only (Fig. 1, C and D). Hook1-positive Rab5 endosomes also showed an increase in retrograde-directed instantaneous velocity as compared with the overall population of Rab5-GFP–positive endosomes (Fig. 1 E). In comparison, Hook1-positive Rab7 endosomes had the same retrograde bias and retrograde-directed instantaneous velocities seen for the overall population of Rab7-GFP endosomes, where ∼50% of organelles displayed fast retrograde motility (Fig. 1, F–H). Overall, this analysis indicates that motile endosomes positive for Hook1 were primarily fast, retrogradely moving organelles, indicative of processive dynein-mediated motility.

Hook1 KD reduces the motility of BDNF-positive signaling endosomes

As Hook1 comigrates with a subpopulation of Rab5- and Rab7-positive endosomes, we next asked whether Hook1 depletion would alter the motility of these endosomes. We used a rat siRNA pool to KD Hook1 in cultured neurons; 60% depletion of Hook1 was observed in PC12 cells using this approach (Fig. S1, G and H). Rab5-GFP or Rab7-GFP was transfected along with Hook1 siRNA and imaged 48 h after transfection at DIV 7–8 along the mid- or distal regions of the axon. Hook1 KD did not induce significant differences in the motile fraction or the directionality of either Rab5- or Rab7-positive endosomes at a population level (Fig. S1, A–F). Hook1 KD did induce a trend toward decreased flux of Rab5 endosomes, but the effect was not significantly different than control (Fig. S1 C).

Olenick et al.
Hook1 activates BDNF-endosome motility

Journal of Cell Biology   221
https://doi.org/10.1083/jcb.201805016

Figure 1. Hook1 comigrates with Rab5 and Rab7 endosomes. (A) Mid-axons of hippocampal neurons expressing Hook1-Halo and Rab5- or Rab7-GFP. Arrows show colocalized Hook1 with the indicated Rab endosome. Bars, 4 µm. **(B)** The percentage of endosomes with Hook1-co-localization. Scatter plot shows mean ± SEM. Rab5: *n* = 17 neurons; Rab7: *n* = 10 neurons. **(C)** Kymograph of Rab5-GFP and Hook1-Halo motility in axon of hippocampal neuron. Arrows show comigrating Hook1-Rab5 organelles. Bars: 4 µm (horizontal); 20 s (vertical). **(D)** The ratio of retrograde to anterograde motility events in neurons expressing Rab5-GFP + Hook1-Halo or Rab5-GFP only. Unpaired *t* test (*, P = 0.0177). Rab5: *n* = 16 neurons; Rab5 + Hk1: *n* = 10 neurons. **(E)** Cumulative histogram of retrograde instantaneous velocities of events in neurons expressing Rab5-GFP + Hook1-Halo or Rab5-GFP only. Dashed line represents one phase decay regression line; half-life (λ) and 95% CI values are shown. **(F)** Kymograph of Rab7-GFP and Hook1-Halo motility in axon of hippocampal neuron. Arrows show comigrating Hook1-Rab7 organelles. Bars: 4 µm (horizontal); 20 s (vertical). **(G)** The ratio of retrograde to anterograde motility events in neurons expressing Rab7-GFP + Hook1-Halo or Rab7-GFP only. Unpaired *t* test (ns, P = 0.8223). Rab7: *n* = 13 neurons; Rab7 + Hk1: *n* = 7 neurons. **(H)** Cumulative histogram of retrograde instantaneous velocities of events in neurons expressing Rab7-GFP + Hook1-Halo or Rab7-GFP only. Dashed line represents one phase decay regression line; half-life(λ) and 95% CI values are shown.

We hypothesized that Hook1 might play a more specific role in the transport of a subpopulation of neuronal endosomes, so we focused on signaling endosomes, which initiate distally and mature through the Rab5 and Rab7 endosomal pathway (Deinhardt et al., 2006; Ye et al., 2018). In neurons, neurotrophic factors such as BDNF bind to their transmembrane kinase receptors and are endocytosed to form signaling endosomes that undergo retrograde transport toward the nucleus, leading to changes in gene expression (Cosker and Segal, 2014; Scott-Solomon and Kuruvilla, 2018). To focus on a signaling endosomal population in neurons, we expressed the neurotrophic receptor TrkB-RFP and GFP-Hook1 and found that the labeled proteins comigrated in the axons of hippocampal neurons (Fig. 2 A). Consistent with this observation, immunoisolation of TrkB vesicles from mouse brain lysates demonstrated the coprecipitation of Hook1 along with subunits of both dynein and dynactin (Fig. S2 A).
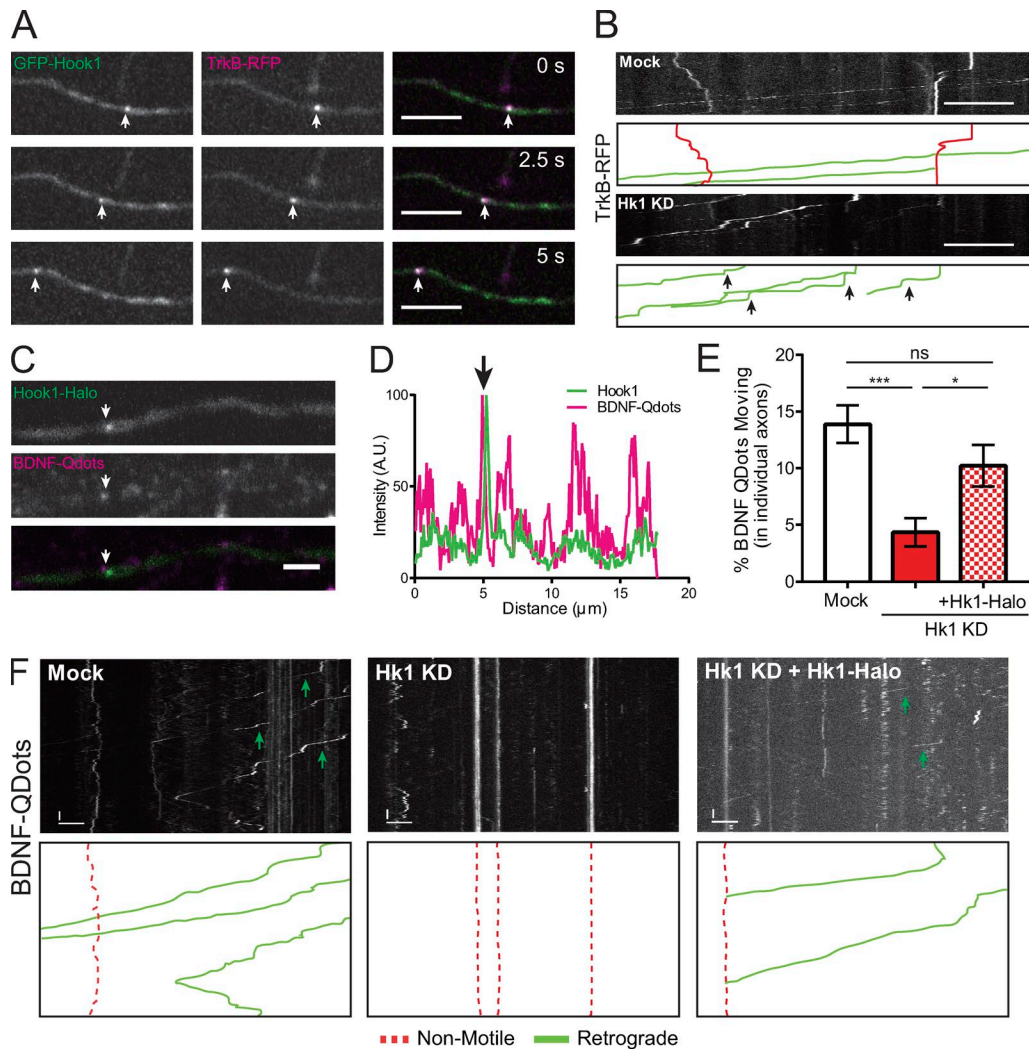
Next, we expressed TrkB-RFP in control and Hook1 KD neurons. Upon Hook1 depletion, retrograde TrkB endosomes displayed less processive motility (as indicated by more pausing [66.6% retrograde events displayed pausing per neuron]) than in control cells (32.2% retrograde events with pausing per neuron; Fig. 2 B). To more directly measure the motility of signaling endosomes, we monitored the uptake and motility of the TrkB ligand BDNF. First, we looked for colocalization of BDNF with Hook1-Halo in neurons. Neurons were serum starved for 1 h, and BDNF-biotin was then added to neuronal cultures for at least 1 h before fixation. Approximately 48% of Hook1-Halo puncta colo-

calized with BDNF–Alexa Fluor 633 in fixed neurons (Fig. S2, B and C). In live neurons, we also found that GFP-Hook1 colocalized with BDNF-conjugated quantum dots (BDNF-Qdots; Fig. 2, C and D). Next, we investigated the motility of BDNF-Qdots in control or Hook1 KD neurons. Neurons with Hook1 KD displayed significantly reduced retrograde BDNF-Qdot motility compared with control neurons (Fig. 2, E and F). This motility defect could be rescued by expression of siRNA-resistant human Hook1-Halo (Fig. 2, E and F).

To assess whether the observed effects of Hook1 depletion were specific for signaling endosomes or instead represented a more generalized inhibition of organelle motility, we imaged mitochondrial motility as well as another highly processive retrograde cargo, LC3B-positive autophagosomes. Comparisons of the motility of mitochondria and autophagosomes in Hook1 KD and control neurons demonstrate that no differences were induced by Hook1 depletion (Fig. S1, G–L). Together with the observations that Hook1 depletion does not induce changes in the motility of the overall population of either Rab5-positive or Rab7-positive endosomes, these results indicate that Hook1 plays an essential and specific role in TrkB–BDNF–signaling endosome motility in axons.

A direct interaction of Hook1 with dynein is important for signaling endosome motility

Dynein subunit LIC1 interacts with several dynein effectors including BICD2, RILP, and FIP3 (Schroeder et al., 2014). Recent

Olenick et al.
Hook1 activates BDNF-endosome motility

Journal of Cell Biology
https://doi.org/10.1083/jcb.201805016

222

Figure 2.   **Hook1 KD reduces TrkB–BDNF-signaling endosome motility. (A)** Time series of the mid-axon of hippocampal neurons expressing GFP-Hook1 and TrkB-RFP. Arrows show retrograde comigration of Hook1 with TrkB vesicles. Bars, 5 µm. **(B)** Kymographs of TrkB-RFP in control or Hk1 KD neurons. Traced events shown below are color-coded for ease of interpretation. Arrows show pausing in retrograde events. Bars, 10 µm; 1 min total. **(C)** Colocalization images of BDNF-Qdots with GFP-Hook1 in the axon of a hippocampal neuron. Arrows show Hook1 puncta colocalized with BDNF. Bar, 2 µm. **(D)** Line scan through axon in C. Arrow points to colocalized Hook1 and BDNF. **(E)** Quantification of BDNF-Qdots motility. Bar graph shows mean ± SEM; Kruskal–Wallis one-way ANOVA (***, P < 0.0001; *, P = 0.030; ns, P = 0.7405). Mock: n = 103 neurons; Hk1 KD: n = 63 neurons; Hk1 KD + Hk1-Halo: n = 55 neurons. **(F)** Kymographs of BDNF-Qdots in control, Hk1 KD, and Hk1 KD + Hk1-Halo neurons. Traced events shown below are color-coded for ease of interpretation. Green arrows indicate retrograde events. Bars: 5 µm (horizontal); 5 s (vertical).

studies have found that the Hook domain conserved in both Hook1 and Hook3 also mediates a direct interaction with LIC1 and is important for Hook-mediated dynein processivity (Schroeder and Vale, 2016; Lee et al., 2018). To determine whether the Hook1–LIC1 interaction is important for signaling endosome motility in neurons, we analyzed two constructs: Hook1(Q149A, I156A), based on previous mutations in Hook3 shown to diminish the interaction with LIC1 (Schroeder and Vale, 2016), and Hook1(M146D, I156D), based on our recent structure of a Hook3–LIC1 complex (Fig. 3, A and B; Lee et al., 2018). We used total internal reflection fluorescence (TIRF) microscopy to perform motility assays with single-molecule resolution to test these mutant constructs and found that both Hook1(Q149A, I156A) and Hook1(M146D, I156D) significantly inhibited dynein-driven motility along microtubules (Fig. 3, C and D).

Next, we tested whether mutating the binding interface of Hook1 and LIC1 would disrupt signaling endosome motility in hippocampal neurons. Similar to our results with Hook1 siRNA KD, BDNF-Qdot motility was significantly reduced in neurons expressing GFP-Hook1(Q149A, I156A) (Fig. 3, E and F). These results indicate that the interaction of Hook1 with LIC1 is important not only for in vitro motility but also during cargo transport of BDNF-signaling endosomes in neurons.

The C-terminal domain of the Hook proteins is thought to specify cargo binding. Comparisons of C-terminal Hook1 sequences from several species identify a high degree of sequence conservation (Fig. S3). There is more limited sequence conservation between Hook1 and Hook3, but we noted that immediately following a conserved sequence there was a pair of charged/polar residues in Hook1 not found within Hook3.
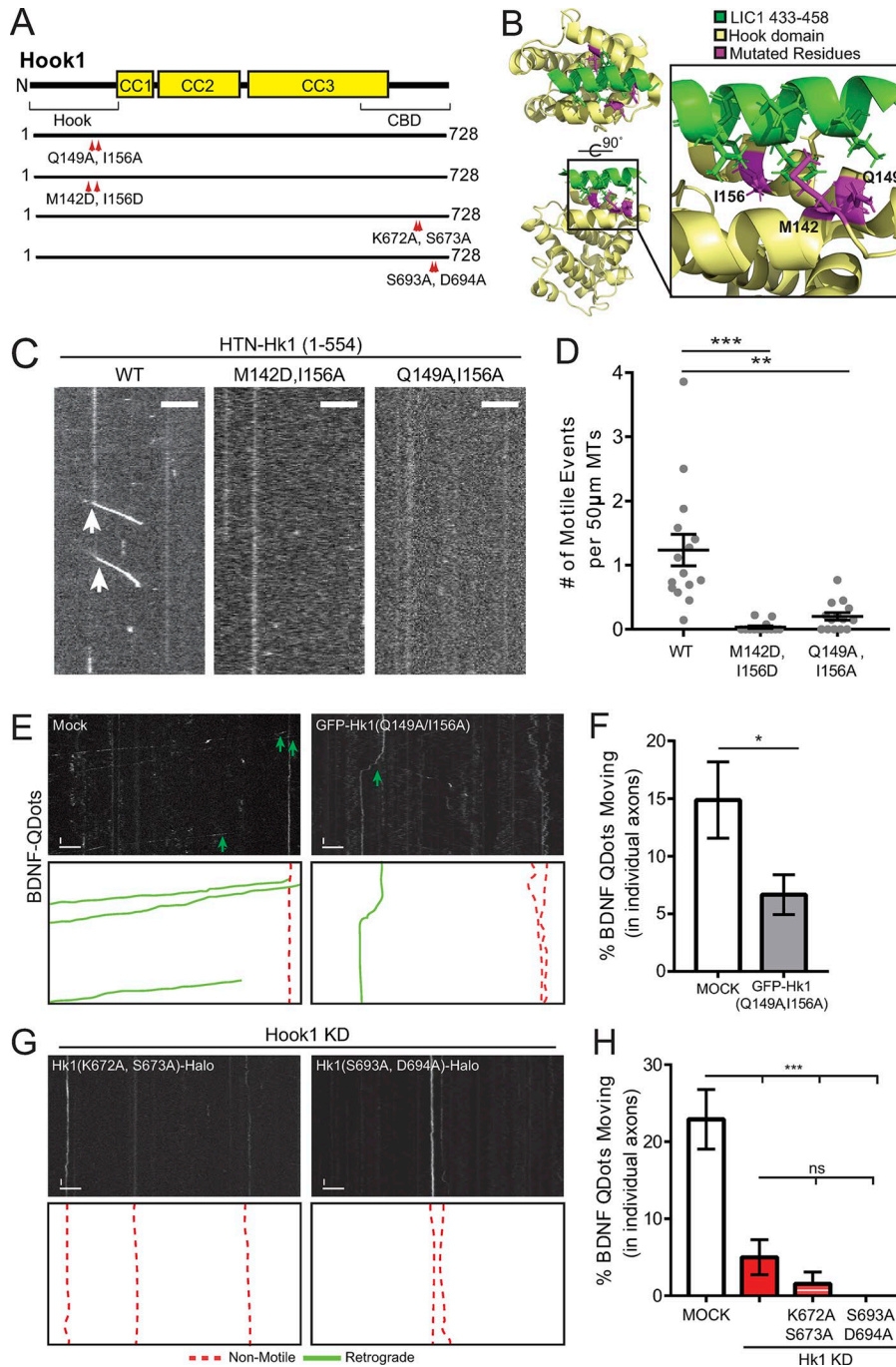
Figure 3. **Hook1 requires interaction with LIC1 for signaling endosome motility. (A)** Diagram of Hook1 domain structure with mutated constructs below. Arrowheads indicate point mutations. **(B)** Hook3 (yellow)–LIC1 helix (green) structure (PDB: 6B9H) with residues that were mutated highlighted in magenta (Hook1 residue numbering). **(C)** Kymographs of Halo-Hook1 constructs from a single-molecule TIRF motility assay. Arrows indicate motile events. Bars, 5 μm; total length, 1 min. **(D)** Quantification of Hook1 motility in a TIRF motility assay. Scatter plot shows mean ± SEM; Kruskal–Wallis one-way ANOVA (***, P < 0.0001; **, P = 0.0012). n = 14–15 videos from three individual experiments. MT, microtubule. **(E)** Kymographs of BDNF-Qdots in axons of hippocampal neurons. Traced events below are color-coded for ease of interpretation. Green arrows indicate retrograde events. **(F)** Quantification of BDNF motility. Bar graph shows mean ± SEM; Mann–Whitney t test (*, P = 0.0262). Mock: n = 31 neurons; Hk1(Q149A, I156A): n = 46 neurons. **(G)** Kymographs of BDNF-Qdots in axons of hippocampal neurons in Hk1 KD-rescue experiments with C-terminal mutated Hook1 constructs. Traced events below are color-coded for ease of interpretation. (E and G) Bars: 5 μm (horizontal); 5 s (vertical). **(H)** Quantification of BDNF motility in KD-rescue experiments. Bar graph shows mean ± SEM; one-way ANOVA (***, P < 0.0001; ns, P = 0.58–0.98). Mock: n = 29 neurons; Hk1 KD: n = 22 neurons; Hk1 KD + Hk1(K672A,S673A): n = 13 neurons; Hk1 KD + Hk1(S693A,D694A): n = 24 neurons.

We engineered a double mutation to generate Halo-tagged Hook1(K672A,S672A) and asked whether this construct could rescue BDNF-Qdot motility in Hook1-depleted neurons. As shown in Fig. 3 G, this construct could not rescue signaling endosome motility. Next, we focused on a 10-aa residue insertion in the C-terminal domain of Hook1 relative to Hook3 and again mutated a pair of polar/charged residues to generate Hook1(S693A, K694A)-Halo. We tested this construct in KD-rescue experiments assaying for BDNF-Qdot motility and found no rescue (Fig. 3 H), further supporting the importance of the C-terminal domain of Hook1 in mediating organelle-specific dynein-driven motility.

Hook1 is enriched in the distal axon and is distinctly localized from other dynein effectors

There are now several dynein effectors implicated in the regulation of dynein-driven motility in cells (Kardon and Vale, 2009; Fu and Holzbaur, 2014; Reck-Peterson et al., 2018). We hypothesized that dynein effectors might display differential localizations in neurons, reflecting distinct roles in intracellular transport. To address this question, we individually expressed Hook1-Halo, RILP-GFP, and BICD2-GFP in hippocampal neurons for 48 h and then fixed the cells on DIV 7–8. Confocal z stacks were captured of the distal axon, mid-axon, and soma of neurons. Images were deconvolved, and the somal localization was scored as either punctate or cytoplasmic.
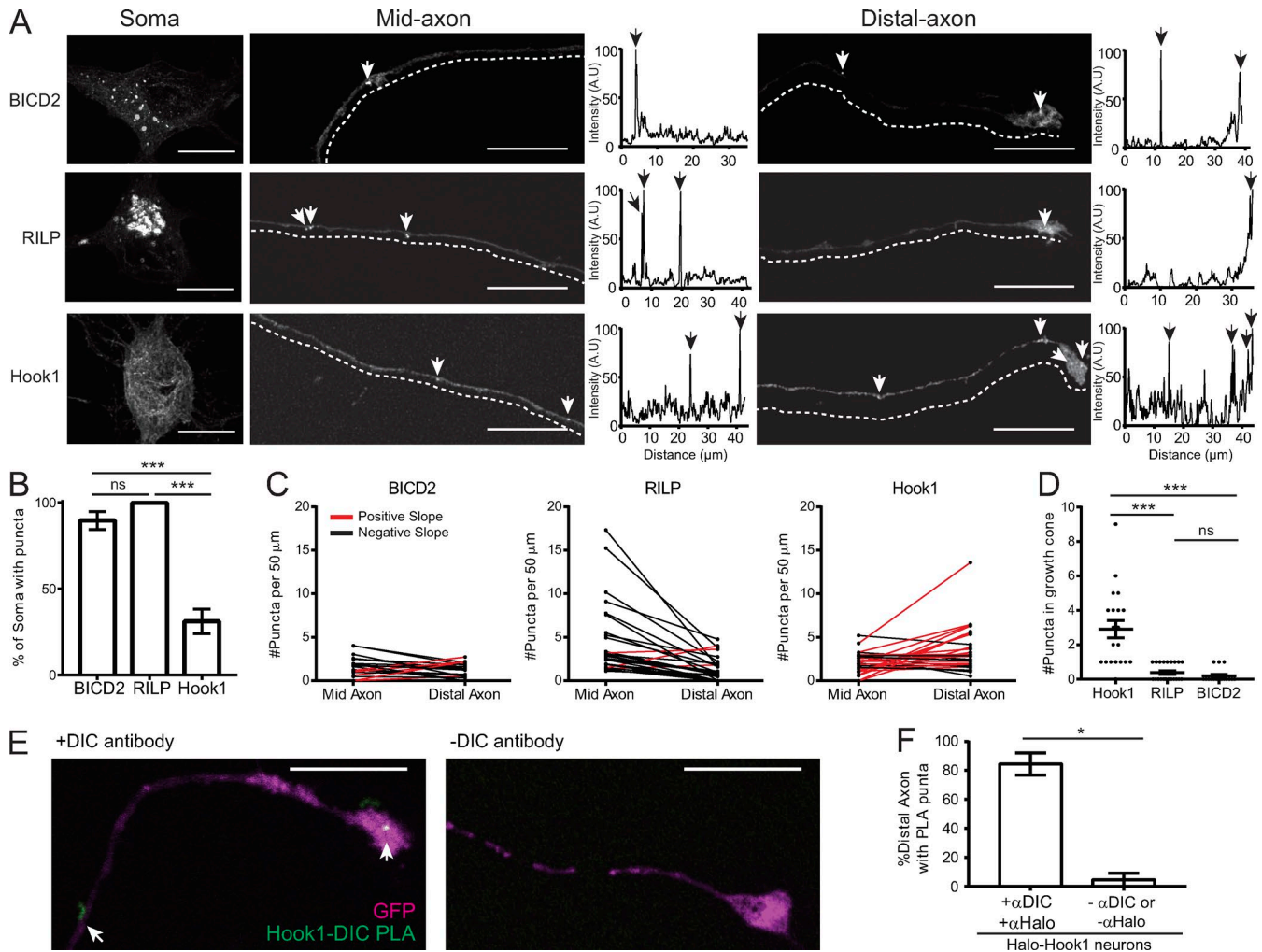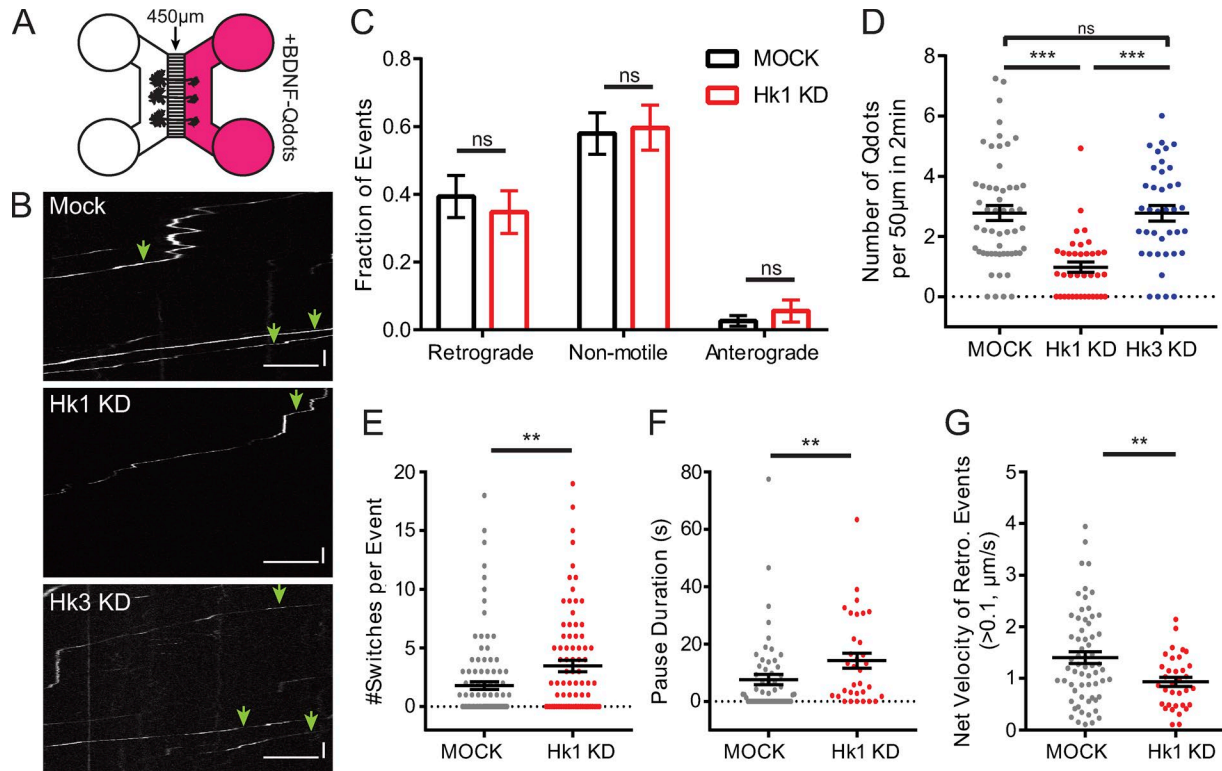
Figure 4. **Hook1 localizes to distal axon, while other dynein effectors are enriched in other compartments. (A)** Representative images of neurons expressing indicated dynein effectors. White arrows point to effector puncta. Dashed line represents the line used for line scan plots , but line is shifted below the axon so as to not obscure primary data. Line scan graphs of mid- and distal axons are shown to the right of the image. Black arrows point to corresponding puncta peaks. **(B)** Quantification of percentage of neurons with puncta in soma. Bar graph shows mean ± SEM; one-way ANOVA (***, P ≤ 0.0001; ns, P = 0.3964). *n* = 3–4 individual experimental averages, 23–26 cells. **(C)** Graphs of dynein effector enrichment in mid versus distal axons. Red lines indicate enrichment in the distal region of axon. Black lines indicate enrichment in the mid-axon. BICD2: *n* = 21 neurons; RILP: *n* = 27 neurons; Hook1: *n* = 27 neurons. **(D)** Graph of dynein effector puncta per growth cone. Scatter plot shows mean ± SEM; one-way ANOVA (***, P < 0.0001; ns, P = 0.8901). *n* = 16–23 growth cones. **(E)** Representative images of proximity ligation assay of Hook1-Halo–expressing distal axons with and without anti-DIC. Hook1–DIC complexes are presented in green and GFP in magenta. Arrow indicates Hook1–DIC complexes. (A and E) Bars, 10 µm. **(F)** Quantification of distal axons with Hook1–DIC PLA puncta present. Bar graph shows mean ± SEM; unpaired *t* test (*, P = 0.0119). *n* = 2 individual experimental averages, 19–38 neurons.

Over 80% of BICD2- and RILP-expressing neurons displayed an accumulation of these effectors in the soma, associated with either large puncta or clusters, while the distribution of Hook1 was predominantly cytoplasmic within the soma (Fig. 4, A and B). In axons, dynein effectors were imaged either in the mid- or distal axon and puncta quantified per unit length, comparing levels along the same axon to assess relative enrichment of individual effectors. BICD2 had a generally sparse distribution in axons compared with RILP and Hook1. In contrast, RILP was enriched in the mid-axon, and Hook1 was enriched in the distal axon (Fig. 4, A and C). We also quantified the density of puncta for each dynein effector within the growth cone and found there was significantly more Hook1 puncta in the growth cone as compared with BICD2 and RILP (Fig. 4 D). The differential localization of these effectors is consistent with their proposed roles in organelle transport. BICD2 is linked to Rab6 ves-

icles (Matanis et al., 2002; Matsuto et al., 2015), which are mainly localized to the soma. RILP is a Rab7 adaptor (Cantalupo et al., 2001; Wu et al., 2005; Johansson et al., 2007; Rocha et al., 2009), and Rab7 vesicles are enriched in the mid-axon and soma. In contrast, the enrichment of Hook1 in the distal axon suggests that this effector is involved early in the pathway of neurotrophic factor uptake and trafficking via signaling endosomes.

To further visualize the Hook1–dynein interaction, we used a proximity ligation assay to image dynein–Hook1 colocalization. Neurons expressing Hook1-Halo were stained with antibodies to the Halo-tag and to endogenous dynein (anti–dynein intermediate chain [DIC]) and visualized using secondary antibodies conjugated to complementary oligonucleotides to visualize complex formation. Using this assay, Hook1–dynein complexes were localized to the distal axon, a distribution not observed in control reactions

Olenick et al.
Hook1 activates BDNF-endosome motility

Journal of Cell Biology
https://doi.org/10.1083/jcb.201805016

225

Figure 5. **Hook1 KD reduces flux of BDNF from distal axon. (A)** Schematic of the microfluidic device and experimental setup. **(B)** Kymographs of BDNF in MOCK, Hk1 KD, and Hk3 KD neurons grown in the microfluidic device. Arrows point to retrograde events. Bars: 10 µm (horizontal); 10 s (vertical). **(C)** Motility fractioned into retrograde, anterograde, and nonmotile events per neuron. Bar graph shows mean ± SEM; two-way ANOVA (ns, P > 0.113) Mock: $n = 35$ neurons; Hk1 KD: $n = 34$ neurons. **(D)** Quantification of flux of BDNF-Qdots in mid-axons. Scatter plot shows mean ± SEM; one-way ANOVA (***, P < 0.0001; ns, P = 0.9994). Mock: $n = 54$ neurons; Hk1 KD: $n = 36$ neurons; Hk3 KD: $n = 29$ neurons. **(E)** Number of switches in BDNF-Qdot events. Scatter plot shows mean ± SEM; Mann–Whitney t test (**, P = 0.001). Mock: $n = 110$ events; Hk1 KD: $n = 84$ events. **(F)** Pause duration of retrograde BDNF-Qdot events. Scatter plot shows mean ± SEM, Mann-Whitney t test (**, P = 0.0062). Mock: $n = 57$ events; Hk1 KD: $n = 33$ events. **(G)** Net velocity of retrograde BDNF-Qdot events. Scatter plot shows mean ± SEM, unpaired t test (**, P = 0.0061). Mock: $n = 63$ events; Hk1 KD: $n = 34$ events.

lacking anti-DIC or anti-Halo antibody (Fig. 4, E and F). In contrast, we did not see the same distal axon signal using the proximity ligation assay to visualize dynein complexed with either RILP or BICD2. These results show that Hook1 is enriched in the distal axon and primed for motility as it is in a complex with dynein.

Hook1 depletion decreases the flux and processivity of BDNF-signaling endosomes from the distal axon

To better model the uptake and transport of BDNF from the distal axon, we used microfluidic devices in which axons grow through microchambers to reach the fluidly isolated axonal chamber, permitting BDNF application only to the distal axons (Fig. 5 A). Hippocampal neurons were electroporated with GFP fill and Hook1 siRNA before plating in the microfluidic devices. Neurons were cultured for 7–8 d, allowing the axons to extend to the distal chamber. Prior to imaging, BDNF-Qdots were added to the axonal chamber of the devices. We compared the motility properties of BDNF-Qdots in Hook1 KD and control neurons (see Videos 1 and 2). While BDNF-Qdots still exhibited a retrograde bias in motility upon Hook1 KD, the flux was greatly reduced compared with control conditions (Fig. 5, B–D). In contrast, neurons transfected with Hook3 siRNA did not show this decrease in BDNF-Qdot flux (Fig. 5 D). In addition to decreased flux, we also noticed a difference in the size of BDNF-Qdot vesicles. Previous research has shown that multiple

neurotrophic factor–bound Qdots may be internalized into a single signaling endosome (Cui et al., 2007). Thus, we measured the apparent size of BDNF-Qdot organelles as a measure of the number of internalized BDNF-Qdots. We found a significant reduction in organelle area in Hook1 KD neurons (0.39 µm², with 0.30–0.48 95% confidence interval [CI]) compared with control neurons (0.62 µm², with 0.51–0.74 95% CI), suggesting less BDNF-Qdots are being endocytosed per vesicle. Overall, this work suggests that Hook1 depletion reduces not only the number of BDNF organelles trafficked down the axon but also the load of individual organelles.

While significantly fewer BDNF-Qdots were observed to traffic along the axon in Hook1-depleted neurons, we analyzed the motility properties of these organelles to see whether loss of the dynein activator would reduce the processivity of signaling endosomes from the distal axon. In Hook1 KD cells, BDNF-Qdots showed less directed motility along the axon, with significantly more directional switching within individual runs (Fig. 5 E). In addition, retrograde events also displayed increased pause duration and reduced net velocity (Fig. 5, F and G). These results suggest that Hook1 does act as a dynein activator to increase the processivity of retrograde BDNF-signaling endosomes once they have been endocytosed.

Since we observed reduced flux and impaired motility of signaling endosomes in Hook1 KD neurons, we hypothesized there
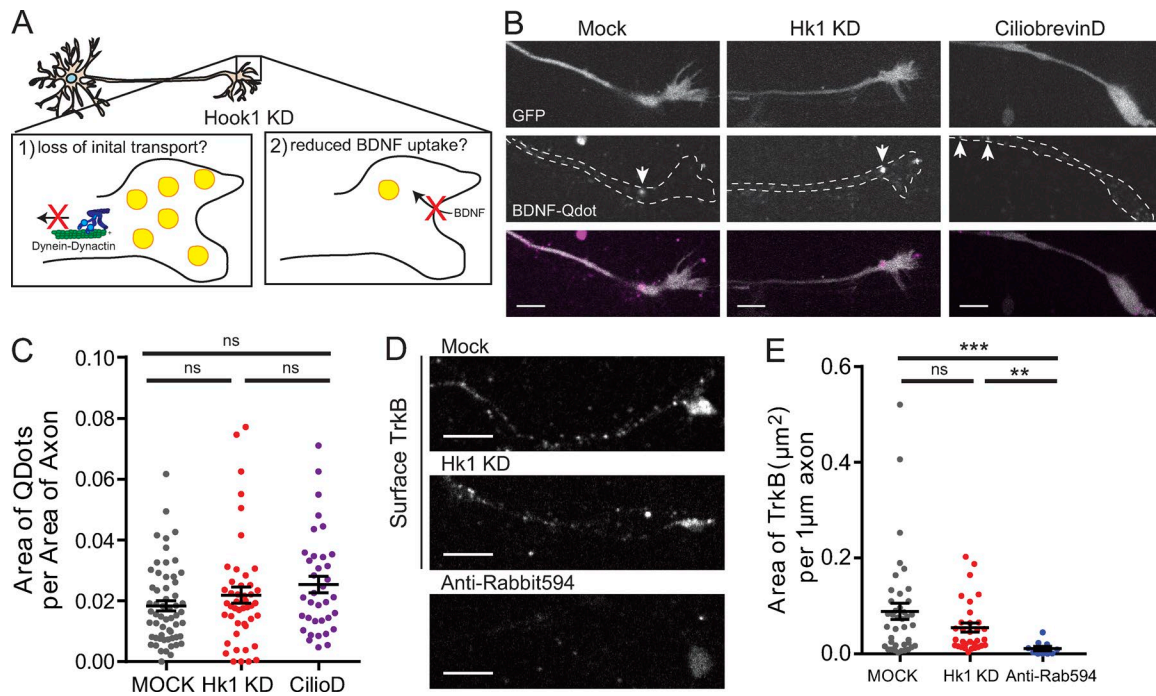
Figure 6. **Impaired signaling endosome motility reduces BDNF endocytosis. (A)** Schematic model of two possible effects of Hook1 KD on distal axons. **(B)** Representative images of distal tips of axons with BDNF-Qdots. Arrows indicate BDNF-Qdots, and the dashed line is the cell outline. **(C)** Area of Qdots in the distal axons normalized by area of axon quantified. Scatter plot shows mean ± SEM; Kruskal–Wallis one-way ANOVA (ns, P > 0.082). Mock: $n = 58$ neurons; Hk1 KD: $n = 46$ neurons; Ciliobrevin D [CilioD]: $n = 3$–6 neurons. **(D)** Surface TrkB staining with anti-TrkB in distal axon of fixed neurons. Bottom panel (anti-Rabbit594) shows the secondary antibody only (as a control). (B and D) Bars, 5 μm. **(E)** Area of surface TrkB per micrometer axonal length. The anti-Rabbit 594 condition is a control for the secondary antibody. Scatter plot shows mean ± SEM; one-way ANOVA (***, P = 0.0004; **, P = 0.0055; ns, P = 0.9741). Mock: $n = 40$ neurons; Hk1 KD: $n = 32$ neurons; anti-Rabbit594: $n = 10$ neurons.

might be a resulting accumulation of BDNF-Qdots at the distal ends of axons due to loss of dynein transport (Fig. 6 A). We imaged the distal regions of axons after several washes to remove excess, surface-associated BDNF-Qdots. Quantification of BDNF-Qdot signal per unit area of axon showed no difference between Hook1 KD and control neurons (Fig. 6, B and C). Similar results were seen when dynein motility was blocked with the dynein inhibitor Ciliobrevin D (Fig. 6, B and C), suggesting there is down-regulation of TrkB endocytosis when motility is impaired, preventing distal accumulation. One way to reduce endocytosis of BDNF is to reduce the amount of its receptor TrkB at the plasma membrane. We measured the amount of plasma membrane–associated TrkB on the surface of Hook1 KD or control axons using an antibody to the TrkB extracellular domain, which is not conserved in other Trk proteins. Neurons were fixed and stained with anti-TrkB (aa 54–67) without permeabilization. There was no significant change in surface TrkB levels at the axon tips with Hook1 depletion, suggesting that a reduction in TrkB levels is not contributing to the reduced flux we observed with Hook1 KD (Fig. 6, D and E). Together, these results suggest that endocytosis of BDNF is down-regulated when dynein motility is impaired, which may constitute a potential mechanism to reduce the distal accumulation of cargos in axons.
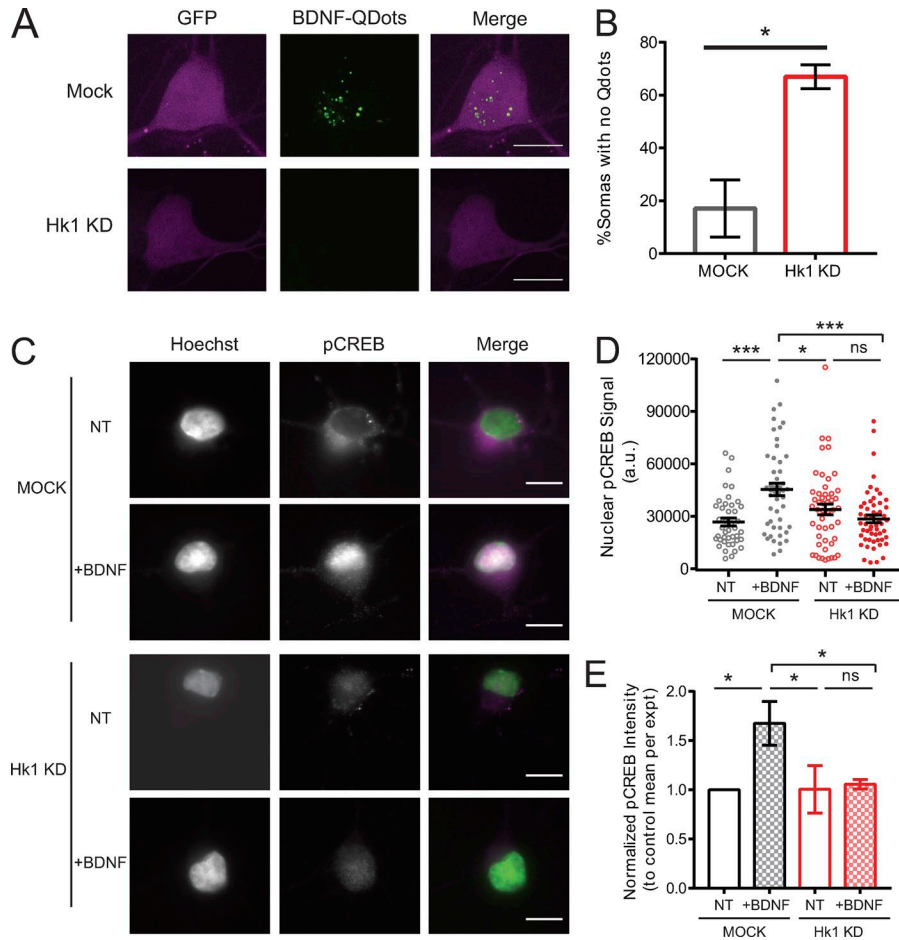
Hook1 KD reduces downstream BDNF signaling to the nucleus
BDNF binds TrkB, which then recruits signaling kinases to produce transcriptional changes in the nucleus (Cosker and Segal, 2014; Mitre et al., 2017). The transport of signaling endosomes

is required to elicit downstream signaling to the nucleus (Ye et al., 2003; Heerssen et al., 2004), so we asked whether loss of Hook1 would affect this signaling pathway due to reduced flux of BDNF. In our Qdot assays, significantly less BDNF-Qdots accumulate in the soma upon Hook1 depletion (Fig. 7, A and B). To measure the downstream signaling, we monitored phosphorylated nuclear cAMP response element–binding protein (CREB), which has been previously shown to increase after treatment with BDNF (Watson et al., 2001). Hook1 KD and control neurons were grown in culture for 7 d in microfluidic devices and then treated with 1 nM BDNF for 1 h before being fixed and stained with anti-pCREB(Ser133) antibody. Using epifluorescence microscopy, we imaged neurons with axons that grew through the microchannels to reach the axonal compartment. In control cells, BDNF-treated neurons had increased nuclear pCREB compared with nontreated (NT) control neurons (Fig. 7, C–E). In Hook1 KD neurons, BDNF-treated cells did not show increased pCREB staining compared with NT cells (Fig. 7, C–E). These results indicate that the reduced flux of BDNF impairs downstream signaling to the nucleus in Hook1-deficient neurons.

Discussion
In this study, we found that Hook1 comigrates with a subpopulation of Rab5- and Rab7-positive endosomes. Previous studies in fungi have implicated Hook proteins in early endosomal transport marked by Rab5, but these systems only express one Hook

Olenick et al.
Hook1 activates BDNF-endosome motility

Journal of Cell Biology 227
https://doi.org/10.1083/jcb.201805016

Figure 7. **Loss of Hook1 leads to loss of downstream signaling measured by pCREB levels.** **(A)** Representative images of somas after BDNF-Qdots treatment. **(B)** Quantification of somas with no BDNF-Qdots present. Bar graph shows mean ± SEM; unpaired *t* test (*, P = 0.0131). *n* = 3 individual experimental averages, 36–41 cells. **(C)** Representative images of soma with pCREB staining. (A and C) Bars, 10 µm. **(D)** Quantification of nuclear pCREB signaling. Scatter plot shows mean ± SEM; one-way ANOVA (*, P = 0.024; ***, P < 0.0002; ns, P = 0.491). Mock, NT: *n* = 42 somas; mock + BDNF: *n* = 48 somas; Hk1 KD, NT: *n* = 51 somas; Hk1 KD + BDNF: *n* = 55 somas. **(E)** Normalized pCREB intensity to the NT mock condition per individual experiment. Bar graph shows mean ± SEM; repeated-measures one-way ANOVA (*, P < 0.047; ns, P = 0.99). *n* = 3 individual experiments.

isoform (Bielska et al., 2014; Zhang et al., 2014). In mammalian systems, Hook1 has been linked to different aspects of the endosomal pathway. In HeLa cells, Hook proteins were found to interact with members of the HOPS complex and to be important for timely trafficking of EGF through endosomal compartments marked by EEA1, CD63, and LAMP1, but this study simultaneously knocked down all three Hook isoforms, making it difficult to determine their individual roles (Xu et al., 2008). Another study using HeLa cells suggested that Hook1 interacts with CD147 to facilitate sorting into Rab22-positive recycling tubules (Maldonado-Báez et al., 2013). In COS-1 cells, Hook1 was found to interact with Rab7, Rab9, and Rab11 using immunoprecipitation (Luiro et al., 2004). The variety of results seen in these studies is likely due to the fluid nature of endosomal pathways and differential cellular demands on these pathways.

In our work, Hook1 comigrates primarily with fast, retrograde Rab5-positive vesicles in primary neurons, which suggests a role for Hook1 in activating the motility of these vesicles. Yet Hook1 depletion produced only subtle effects on the dynamics of the total Rab5-positive endosomal population in axons, significantly affecting only signaling endosome motility, suggesting a higher level of specificity than previously observed for dynein effectors that interact directly with Rab proteins such as the interaction of BICD proteins with Rab6 (Schlager et al., 2010; Matsuto et al., 2015; Terawaki et al., 2015; Huynh and Vale, 2017) or RILP with Rab7 (Cantalupo et al., 2001; Wu et al., 2005; Johansson et

al., 2007). Instead of cargo attachment through a Rab protein, Hook1 has been suggested to attach to cargo through C-terminal interactions with Fused Toes (FTS) and FTS-Hook interacting (FHIP) proteins (Xu et al., 2008; Yao et al., 2014; Guo et al., 2016). It remains to be determined whether Hook1 is linked to signaling endosomes by FTS–FHIP or another protein complex in neuronal systems. Of note, mutating pairs of residues conserved within the C-terminal domain of Hook1, but not found in Hook3, was sufficient to disrupt the ability of Hook1 to activate the transport of signaling endosomes (Fig. 3, G and H), supporting a key role for the C-terminal of Hook1 in mediating organelle-specific dynein-driven motility.

In this study, we found that Hook1 plays a role in signaling endosome processivity. Our previous work has shown that Hook1 increases dynein-dynactin processivity in vitro, with Hook1-bound dynein displaying higher velocities and longer run lengths than BICD2-associated motors (Olenick et al., 2016). Recent cryo-EM structures have shown Hook3 can recruit two dynein dimers per dynactin complex (Urnavicius et al., 2018). Due to the high sequence similarity in the Hook domain and coiled-coil regions, it is likely that Hook1 functions in a similar manner. It is possible that the relatively high velocities observed for signaling endosome transport (averaging 1.4 µm/s) are due to the incorporation of two dynein dimers into the dynein–dynactin–Hook1 complex.

We also found that the interaction of Hook1 with dynein subunit LIC1 is essential for signaling endosome motility, a mechanism
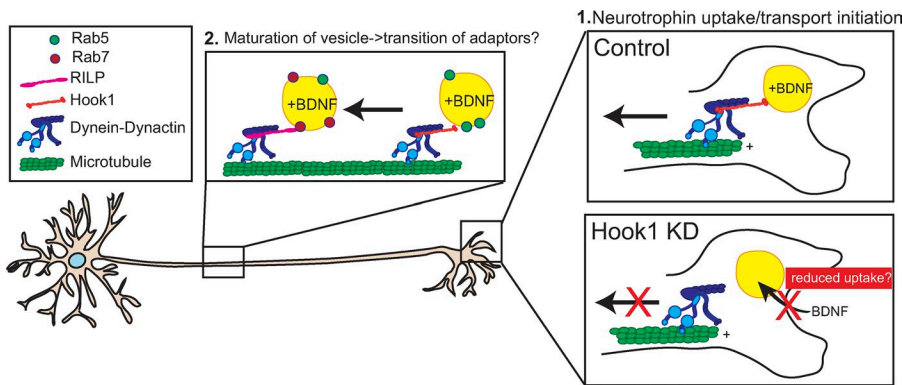
Figure 8. **Model of neurotrophin uptake and transport from distal axon.** In our model, Hook1 plays a role in early dynein-mediated transport of BDNF-TrkB signaling endosomes. As signaling endosomes are transported to the soma, there might be handoff or exchange of dynein effectors as the vesicles mature from Rab5 to Rab7 positive.

that is likely conserved in other dynein effectors regulating cargo transport in the cell. Recent structural work showed that a helix (aa 433–458) within the otherwise unstructured C-terminal region of LIC1 is a conserved interface for the binding of dynein effectors including BICD2, Spindly, and Hook proteins (Lee et al., 2018). Since the LIC1 interaction region is conserved among dynein effectors, it is likely that competition for this binding site plays a role in regulating cargo transport. During our investigation of Hook1, we observed differential localization of the dynein effectors Hook1, BICD2, and RILP in hippocampal neurons. It is possible that the compartmentalization of neurons and the differential localization of dynein effectors locally regulates the competition of dynein effectors for dynein–dynactin binding sites.

In this study, we found that Hook1 plays a key role early in the transport of TrkB–BDNF endosomes as reflected by Hook1 enrichment in the distal axon. This enrichment is not seen for RILP or BICD2. In contrast, RILP was enriched in the mid-axon and soma, consistent with its role in mediating Rab7-endosome motility (Cantalupo et al., 2001; Johansson et al., 2007). It remains to be investigated whether there is a transition or handoff of dynein effectors during endosomal maturation and conversion from Rab5- to Rab7-positive organelles (Fig. 8) in line with the key role proposed for Rab7-positive multivesicular bodies in mediating the long-distance trafficking of TrkA in sympathetic neurons (Ye et al., 2018). It is also possible that a given cargo could have a mixture of dynein effectors. While Hook and BICD proteins are dynein effectors that modulate dynein processivity, there is as yet no direct evidence of RILP acting as a dynein activator, but other studies have shown that it acts as an adaptor to recruit dynein to Rab7 cargo (Johansson et al., 2007; Rocha et al., 2009). Similarly, Snapin has been reported to recruit dynein to BDNF–TrkB-positive signaling endosomes (Zhou et al., 2012), although this protein lacks the secondary structure expected for a dynein activator (Reck-Peterson et al., 2018). It is possible that a complement of dynein effectors and activators may be required to effectively recruit motors and activate transport; it remains to be seen whether there is coordination between dynein activators and adaptors to help maintain a constant processive dynein pool on a given organelle.

Using microfluidic devices, we showed that loss of Hook1 reduces the flux and processivity of BDNF-signaling endosomes. However, this reduced flux to the cell body did not result in an accumulation of BDNF-Qdots in the distal axon. Similarly, inhibiting dynein motility with Ciliobrevin D also did not lead to the accumulation of BDNF-Qdot levels in the distal axon, suggesting that endocytosis is down-regulated when endosomal motility is inhibited. BDNF has been reported to be a self-amplifying autocrine factor, which can signal to promote BDNF expression and increase TrkB membrane levels (Cheng et al., 2011). Therefore, loss of BDNF signaling could reduce TrkB surface levels and regulate endocytosis to prevent a buildup of BDNF endosomes at the distal tip. However, we detected no significant change in plasma membrane–associated TrkB levels at the axon tip upon Hook1 depletion, suggesting that another mechanism might be at work. An alternative possibility is that the internalization of the TrkB–BDNF complex via endocytosis is tightly linked to the formation of a high-speed, highly processive Hook1-dependent transport compartment. Thus, if transport is blocked either by Hook1 depletion or dynein inhibition, internalization may also be down-regulated, preventing the distal accumulation of stalled signaling endosomes. Hook1 binding partners such as FTS and FHIP proteins (Xu et al., 2008; Yao et al., 2014; Guo et al., 2016) may mediate this coordination of uptake and transport, an interesting question for future studies.

TrkB–BDNF signaling is important for neuronal survival, and disruption of signaling endosome trafficking has been found in models of neurodegenerative diseases including Huntington's or Parkinson's disease (Millecamps and Julien, 2013). In Huntington's disease, the polyQ-expanded huntingtin protein has been shown to impair BDNF retrograde trafficking, leading to reduced neuronal survival (Gauthier et al., 2004). α-Synuclein has also been shown to impair BDNF transport in a mouse model of Parkinson's disease (Fang et al., 2017). Currently, it is unclear whether Hook proteins play a role in these neurodegenerative diseases, but Hook1 and Hook3 have been localized to tau aggregates, a pathological hallmark of Alzheimer's disease, frontotemporal dementia, and other tauopathies (Herrmann et al., 2015). With our new understanding of Hook1 as a dynein effector for BDNF transport in nonpathological states, the role of Hook1 in disease states can now be investigated in more detail in future studies.

Materials and methods
Plasmids and reagents
Halo-tagged Hook1 constructs were generated from the human Hook1 sequence (UniProt code Q9UJC3) and using the HaloTag from the pHTN or pHTC Halo tag CMV-neo vector (Promega).

Olenick et al.
Hook1 activates BDNF-endosome motility

Journal of Cell Biology 229
https://doi.org/10.1083/jcb.201805016

GFP-Hook1 constructs were generated in the pEGFP vector. Rab5-GFP was provided by M. Zerial (Max Planck Institute, Dresden, Germany). Rab7-GFP was purchased from Addgene. TrkB-mRFP was provided by M. Chao (New York University, New York, NY). RILP-GFP was provided by J. Neefjes (Leiden University Medical Center, Leiden, Netherlands). BICD2-GFP was provided by A. Akhmanova (Utrecht University, Utrecht, Netherlands). Empty pEGFP-N1 (Addgene) was used as a cell fill to identify neuronal morphology.

Antibodies used for biochemistry and Western blotting included anti-Hook1 (rabbit; 1:250; ab104514; for detection of rat protein; Abcam), anti-Hook1 (rabbit; 1:500; ab150397; for detection of mouse protein; Abcam), anti-Hook3 (rabbit; 1:1,000; ProteinTech), anti-actin (mouse; 1:1,000; EMD Millipore), anti-DIC (mouse; 1:1,000; EMD Millipore), anti-TrkB (rabbit; 1:4,000; ab187041; Abcam), and anti-Halo (rabbit; Promega). For immunofluorescence experiments, anti-pCREB(Ser133) (rabbit; 1:1,000; Cell Signaling) and anti-TrkB (aa 55–67; rabbit; 1:1,000; EMD Millipore) were used. For TIRF assays, the monoclonal antibody used was anti–β-tubulin (1:40; mouse; T5201; Sigma-Aldrich). An ON-TARGETplus siRNA SMARTpool of four siRNAs for rat Hook1 or Hook3 was purchased from GE Healthcare.

Neuronal culture
E18 Sprague–Dawley rat hippocampal neurons were obtained in suspension from the Neuron Culture Service Center at the University of Pennsylvania and plated on 35-mm glass-bottom dishes (MatTek) or 25-mm coverslips (World Precision). Dishes or coverslips were precoated with 0.5 mg/ml poly-L-lysine (Sigma-Aldrich) 24 h before plating. Neurons were cultured at 37°C with 5% CO_2 in maintenance media that consisted of Neurobasal (Gibco) supplemented with 2 mM GlutaMAX, 100 U/ml penicillin, 100 mg/ml streptomycin, and 2% B27 (Thermo Fisher Scientific). Every 3–4 d, 40% of the media was replaced with fresh maintenance media supplemented with 1 µM AraC.

Neuronal imaging
Imaging was done at DIV 7–8 with neurons transfected 24–48 h before imaging. Neurons were transfected using Lipofectamine 2000 (Invitrogen) according to the manufacturer's instructions, with 0.3–1 µg of each DNA plasmid and, for siRNA conditions, 45 pmol siRNA. Control siRNA labeled with Cy5 was used to confirm transfection of siRNA with Lipofectamine in cultured neurons. Neurons were imaged in low-fluorescence media (HibernateE; Brain Bits) supplemented with 2% B27 and 1% GlutaMAX. For experiments with Halo-Tag constructs, neurons were labeled with tetramethyl rhodamine (TMR) Halo-Tag ligands according to the manufacturer's instructions (Promega). For mitochondria imaging, TMR ethyl ester (TMRE) was added according to manufacturer's protocol. Neurons were imaged in an environmental chamber at 37°C on a spinning-disk confocal UltraView VOX (PerkinElmer) on an inverted Nikon Eclipse Ti microscope with the Prefect Focus system using Apochromat 100× 1.49 NA oil-immersion objective and a C9100-50 electron-multiplying charge-coupled device camera (Hamamatsu Photonics) controlled by Volocity software (PerkinElmer). Axons and dendrites were identified based on morphological criteria as outlined elsewhere (Kaech and Banker, 2006). The distal axon is defined as the area <100 µm from the axon terminal, while the mid-axon is defined as the area >100 µm from the axon terminal and >100 µm from the soma.

Microfluidic experiments
Round microfluidic devices of 450 µm (Xona microfluidics) were used for axon isolation experiments. Devices were UV sterilized and attached to poly-L-lysine–coated imaging dishes (Fluoro-Dish; World Precision Instruments) before plating. On the day of plating, neurons were nucleofected with an Amaxa Nucleofector machine (Lonza) with DNA/siRNA in similar quantities as described above. Cells were plated to one side of microfluidic device at 4×10^5 cells per dish. Fresh maintenance media was added every 2 d (∼30%).

BDNF-Qdot experiments
Neurons were serum starved in unsupplemented Neurobasal (Gibco) for 2–4 h before BDNF-Qdot addition. 50 nM hBDNF-biotin (Alomone Labs) was combined with 50 nM Quantum Dot ITK 655 Streptavidin conjugate (Invitrogen) for 1 h on ice to generate BDNF-Qdots. After conjugation, BDNF-Qdots were added to neurons in unsupplemented Neurobasal to a final concentration of 0.25 nM for 1–2 h. In microfluidic experiments, BDNF-Qdots were only added to the axon side. For pCREB experiments, 1 nM unconjugated BDNF-biotin was added for 1 h before fixing. For Ciliobrevin D (EMD Millipore) conditions, 20 µM Ciliobrevin D was added 10 min before BDNF-Qdot addition and was present throughout BDNF-Qdot treatment and imaging, with the same timescale as control conditions.

Immunofluorescence
Neurons cultured on 25-mm glass coverslips were fixed at DIV 7–8 in PBS containing 4% paraformaldehyde and 4% sucrose for 8 min. Coverslips were washed three times in PBS and blocked with cell block (PBS with 5% normal goat serum and 1% BSA). Primary antibodies were incubated for 2 h at RT in cell block. After removing the primary antibodies, the coverslips were washed with PBS and incubated for 1 h at RT with fluorophore-conjugated secondary antibodies diluted in cell block. Following washes with PBS, the coverslips were mounted in ProLong Gold Antifade Mountant (Thermo Fisher Scientific) on glass slides. For proximity ligation assays, Duolink PLA kit with red detection reagents was used according to manufacturer's protocol (Sigma-Aldrich).

TIRF motility assay
Single-molecule TIRF motility assays were performed as previously described in detail (Olenick et al., 2016). In brief, HeLa cells 18–20 h after transfection of Halo-Hook1 constructs were labeled with the Halo ligand TMR (Promega) and lysed in buffer containing 40 mM Hepes, 1 mM EDTA, 120 mM NaCl, 0.1% Triton X-100, and 1 mM magnesium ATP, pH 7.4, supplemented with protease inhibitors. Cell lysates were diluted in assay buffer containing 10 mM magnesium ATP, 0.3 mg/ml BSA, 0.3 mg/ml casein, 10 mM DTT, and an oxygen-scavenging system. Diluted cell lysates were then flowed into imaging chambers with Taxol-stabilized microtubules immobilized to the coverslip with a tu-

bulin antibody. TIRF videos were acquired at RT at four frames per second using the Nikon TIRF system (Perkin Elmer) on an inverted Ti microscope with a 100× objective and an ImageEM C9100–13 camera (Hamamatsu Photonics) controlled by Volocity software.

Immunoisolation of TrkB vesicles
Using three mouse brains per immunoprecipitation experiment, lysates were homogenated in Hepes buffer (10 mM Hepes, pH 7.4, 1 mM EDTA, and protease inhibitors) and then centrifuged at 800× g for 10 min and 3,000× g for 10 min. The supernatant was then added to Dynabeads protein G (Thermo Fisher Scientific) with anti-TrkB (Abcam) or anti-Halo (Promega) as a rabbit IgG control. Lysates were incubated for 15 min at RT and then washed three times with Hepes buffer. Proteins were then eluted in denaturing buffer and boiled 5 min before running on a SDS-PAGE gel.

Western blotting
To test siRNA efficiency, PC12 cells were transfected at 70–80% confluency with 45 pmol of a pool of Hook1 or Hook3 siRNAs using Lipofectamine RNAiMAX (Invitrogen) and lysed 48 h later. PC12 cells were lysed (50 mM Tris-HCl, pH 7.4, 150 mM NaCl, 1% Triton-X100, and protease inhibitors) and clarified by centrifugation at 13,200 rpm for 10 min at 4°C. For all Western blot experiments, samples were boiled in denaturing buffer for 5 min and run on a SDS-PAGE gel to separate proteins.

Imaging analysis
For motility analysis, kymographs were generated using the MultipleKymograph plugin for Fiji (ImageJ; National Institutes of Health) and analyzed using custom MATLAB software (MathWorks) or by measurement tools in Fiji. For effector localization, images were deconvolved using Huygens Professional software. Effector puncta were then counted by hand, and axon length was measured in Fiji. Area of BDNF-Qdot was measured using measurement and analysis functions in Volocity. The pCREB signal was measured by outlining the nucleus with a Hoechst stain and measuring the integrated intensity of pCREB in that area with Fiji.

Statistical methods
Statistics were performed in GraphPad Prism. A Student's t test or Mann–Whitney test was used when comparing two datasets as indicated, while a ANOVA was used with multiple datasets. For all experiments, data were analyzed from at least three independent replicates. Statistical significance is noted as follows: NS, P > 0.05; *, P ≤ 0.05; **, P ≤ 0.01; and ***, P ≤ 0.001. Figure legends contain specific P value for that figure.

Online supplemental materials
Fig. S1 shows that Hook1 KD does not significantly change Rab5, Rab7, mitochondria, or autophagosome motility. Fig. S2 shows that Hook1 is present on TrkB-BDNF vesicles using biochemistry and imaging. Fig. S3 is the sequence analysis of Hook1 and Hook3 C terminus that informed design of mutant constructs. Video 1 shows BDNF-Qdots motility in control neurons grown in micro-

fluidic chambers. Video 2 shows BDNF-Qdots motility in Hk1 KD neurons grown in microfluidic chambers.

References
Ayloo, S., J.E. Lazarus, A. Dodda, M. Tokito, E.M. Ostap, and E.L.F. Holzbaur. 2014. Dynactin functions as both a dynamic tether and brake during dynein-driven motility. *Nat. Commun.* 5:4807. https://doi.org/10.1038/ncomms5807

Bielska, E., M. Schuster, Y. Roger, A. Berepiki, D.M. Soanes, N.J. Talbot, and G. Steinberg. 2014. Hook is an adapter that coordinates kinesin-3 and dynein cargo attachment on early endosomes. *J. Cell Biol.* 204:989–1007. https://doi.org/10.1083/jcb.201309022

Cantalupo, G., P. Alifano, V. Roberti, C.B. Bruni, and C. Bucci. 2001. Rab-interacting lysosomal protein (RILP): the Rab7 effector required for transport to lysosomes. *EMBO J.* 20:683–693. https://doi.org/10.1093/emboj/20.4.683

Cheng, P.-L., A.-H. Song, Y.-H. Wong, S. Wang, X. Zhang, and M.-M. Poo. 2011. Self-amplifying autocrine actions of BDNF in axon development. *Proc. Natl. Acad. Sci. USA.* 108:18430–18435. https://doi.org/10.1073/pnas.1115907108

Chowdhury, S., S.A. Ketcham, T.A. Schroer, and G.C. Lander. 2015. Structural organization of the dynein-dynactin complex bound to microtubules. *Nat. Struct. Mol. Biol.* 22:345–347. https://doi.org/10.1038/nsmb.2996

Cosker, K.E., and R.A. Segal. 2014. Neuronal signaling through endocytosis. *Cold Spring Harb. Perspect. Biol.* 6:a020669. https://doi.org/10.1101/cshperspect.a020669

Cui, B., C. Wu, L. Chen, A. Ramirez, E.L. Bearer, W.-P. Li, W.C. Mobley, and S. Chu. 2007. One at a time, live tracking of NGF axonal transport using quantum dots. *Proc. Natl. Acad. Sci. USA.* 104:13666–13671. https://doi.org/10.1073/pnas.0706192104

Deinhardt, K., S. Salinas, C. Verastegui, R. Watson, D. Worth, S. Hanrahan, C. Bucci, and G. Schiavo. 2006. Rab5 and Rab7 control endocytic sorting along the axonal retrograde transport pathway. *Neuron.* 52:293–305. https://doi.org/10.1016/j.neuron.2006.08.018

Fang, F., W. Yang, J.B. Florio, E. Rockenstein, B. Spencer, X.M. Orain, S.X. Dong, H. Li, X. Chen, K. Sung, et al. 2017. Synuclein impairs trafficking and signaling of BDNF in a mouse model of Parkinson's disease. *Sci. Rep.* 7:3868. https://doi.org/10.1038/s41598-017-04232-4

Fu, M.-M., and E.L.F. Holzbaur. 2014. Integrated regulation of motor-driven organelle transport by scaffolding proteins. *Trends Cell Biol.* 24:564–574. https://doi.org/10.1016/j.tcb.2014.05.002

Gauthier, L.R., B.C. Charrin, M. Borrell-Pagès, J.P. Dompierre, H. Rangone, F.P. Cordelières, J. De Mey, M.E. MacDonald, V. Lessmann, S. Humbert, and F. Saudou. 2004. Huntingtin controls neurotrophic support and survival of neurons by enhancing BDNF vesicular transport along microtubules. *Cell.* 118:127–138. https://doi.org/10.1016/j.cell.2004.06.018

Grotjahn, D.A., S. Chowdhury, Y. Xu, R.J. McKenney, T.A. Schroer, and G.C. Lander. 2018. Cryo-electron tomography reveals that dynactin recruits a team of dyneins for processive motility. *Nat. Struct. Mol. Biol.* 25:203–207. https://doi.org/10.1038/s41594-018-0027-7

Guo, X., G.G. Farías, R. Mattera, and J.S. Bonifacino. 2016. Rab5 and its effector FHF contribute to neuronal polarity through dynein-dependent retrieval of somatodendritic proteins from the axon. *Proc. Natl. Acad. Sci. USA.* 113:E5318–E5327. https://doi.org/10.1073/pnas.1601844113

Guthrie, C.R., G.D. Schellenberg, and B.C. Kraemer. 2009. SUT-2 potentiates tau-induced neurotoxicity in Caenorhabditis elegans. *Hum. Mol. Genet.* 18:1825–1838. https://doi.org/10.1093/hmg/ddp099

Heerssen, H.M., M.F. Pazyra, and R.A. Segal. 2004. Dynein motors transport activated Trks to promote survival of target-dependent neurons. *Nat. Neurosci.* 7:596–604. https://doi.org/10.1038/nn1242

Herrmann, L., C. Wiegmann, A. Arsalan-Werner, I. Hilbrich, C. Jäger, K. Flach, A. Suttkus, I. Lachmann, T. Arendt, and M. Holzer. 2015. Hook proteins: association with Alzheimer pathology and regulatory role of hook3 in amyloid beta generation. *PLoS One.* 10:e0119423. https://doi.org/10.1371/journal.pone.0119423

Huynh, W., and R.D. Vale. 2017. Disease-associated mutations in human BICD2 hyperactivate motility of dynein-dynactin. *J. Cell Biol.* 216:3051–3060. https://doi.org/10.1083/jcb.201703201

Johansson, M., N. Rocha, W. Zwart, I. Jordens, L. Janssen, C. Kuijl, V.M. Olkkonen, and J. Neefjes. 2007. Activation of endosomal dynein motors by stepwise assembly of Rab7-RILP-p150Glued, ORP1L, and the receptor betalll spectrin. *J. Cell Biol.* 176:459–471. https://doi.org/10.1083/jcb.200606077

Kaech, S., and G. Banker. 2006. Culturing hippocampal neurons. *Nat. Protoc.* 1:2406–2415. https://doi.org/10.1038/nprot.2006.356

Kardon, J.R., and R.D. Vale. 2009. Regulators of the cytoplasmic dynein motor. *Nat. Rev. Mol. Cell Biol.* 10:854–865. https://doi.org/10.1038/nrm2804

Lee, I.-G., M.A. Olenick, M. Boczkowska, C. Franzini-Armstrong, E.L.F. Holzbaur, and R. Dominguez. 2018. A conserved interaction of the dynein light intermediate chain with dynein-dynactin effectors necessary for processivity. *Nat. Commun.* 9:986. https://doi.org/10.1038/s41467-018-03412-8

Luiro, K., K. Yliannala, L. Ahtiainen, H. Maunu, I. Järvelä, A. Kyttälä, and A. Jalanko. 2004. Interconnections of CLN3, Hook1 and Rab proteins link Batten disease to defects in the endocytic pathway. *Hum. Mol. Genet.* 13:3017–3027. https://doi.org/10.1093/hmg/ddh321

Maday, S., A.E. Twelvetrees, A.J. Moughamian, and E.L.F. Holzbaur. 2014. Axonal transport: cargo-specific mechanisms of motility and regulation. *Neuron.* 84:292–309. https://doi.org/10.1016/j.neuron.2014.10.019

Maldonado-Báez, L., N.B. Cole, H. Krämer, and J.G. Donaldson. 2013. Microtubule-dependent endosomal sorting of clathrin-independent cargo by Hook1. *J. Cell Biol.* 201:233–247. https://doi.org/10.1083/jcb.201208172

Matanis, T., A. Akhmanova, P. Wulf, E. Del Nery, T. Weide, T. Stepanova, N. Galjart, F. Grosveld, B. Goud, C.I. De Zeeuw, et al. 2002. Bicaudal-D regulates COPI-independent Golgi-ER transport by recruiting the dynein-dynactin motor complex. *Nat. Cell Biol.* 4:986–992. https://doi.org/10.1038/ncb891

Matsuto, M., F. Kano, and M. Murata. 2015. Reconstitution of the targeting of Rab6A to the Golgi apparatus in semi-intact HeLa cells: A role of BICD2 in stabilizing Rab6A on Golgi membranes and a concerted role of Rab6A/BICD2 interactions in Golgi-to-ER retrograde transport. *Biochim. Biophys. Acta.* 1853(10, 10 Pt A):2592–2609. https://doi.org/10.1016/j.bbamcr.2015.05.005

McKenney, R.J., W. Huynh, M.E. Tanenbaum, G. Bhabha, and R.D. Vale. 2014. Activation of cytoplasmic dynein motility by dynactin-cargo adapter complexes. *Science.* 345:337–341. https://doi.org/10.1126/science.1254198

Millecamps, S., and J.-P. Julien. 2013. Axonal transport deficits and neurodegenerative diseases. *Nat. Rev. Neurosci.* 14:161–176. https://doi.org/10.1038/nrn3380

Mitre, M., A. Mariga, and M.V. Chao. 2017. Neurotrophin signalling: novel insights into mechanisms and pathophysiology. *Clin. Sci. (Lond.).* 131:13–23. https://doi.org/10.1042/CS20160044

Moynihan, K.L., R. Pooley, P.M. Miller, I. Kaverina, and D.M. Bader. 2009. Murine CENP-F regulates centrosomal microtubule nucleation and

interacts with Hook2 at the centrosome. *Mol. Biol. Cell.* 20:4790–4803. https://doi.org/10.1091/mbc.e09-07-0560

Olenick, M.A., M. Tokito, M. Boczkowska, R. Dominguez, and E.L.F. Holzbaur. 2016. Hook Adaptors Induce Unidirectional Processive Motility by Enhancing the Dynein-Dynactin Interaction. *J. Biol. Chem.* 291:18239–18251. https://doi.org/10.1074/jbc.M116.738211

Reck-Peterson, S.L., A. Yildiz, A.P. Carter, A. Gennerich, N. Zhang, and R.D. Vale. 2006. Single-molecule analysis of dynein processivity and stepping behavior. *Cell.* 126:335–348. https://doi.org/10.1016/j.cell.2006.05.046

Reck-Peterson, S.L., W.B. Redwine, R.D. Vale, and A.P. Carter. 2018. The cytoplasmic dynein transport machinery and its many cargoes. *Nat. Rev. Mol. Cell Biol.* 1. https://doi.org/10.1038/s41580-018-0004-3

Redwine, W.B., M.E. DeSantis, I. Hollyer, Z.M. Htet, P.T. Tran, S.K. Swanson, L. Florens, M.P. Washburn, and S.L. Reck-Peterson. 2017. The human cytoplasmic dynein interactome reveals novel activators of motility. *eLife.* 6:e28257. https://doi.org/10.7554/eLife.28257

Rocha, N., C. Kuijl, R. van der Kant, L. Janssen, D. Houben, H. Janssen, W. Zwart, and J. Neefjes. 2009. Cholesterol sensor ORP1L contacts the ER protein VAP to control Rab7-RILP-p150 Glued and late endosome positioning. *J. Cell Biol.* 185:1209–1225. https://doi.org/10.1083/jcb.200811005

Ross, J.L., K. Wallace, H. Shuman, Y.E. Goldman, and E.L.F. Holzbaur. 2006. Processive bidirectional motion of dynein-dynactin complexes in vitro. *Nat. Cell Biol.* 8:562–570. https://doi.org/10.1038/ncb1421

Schlager, M.A., L.C. Kapitein, I. Grigoriev, G.M. Burzynski, P.S. Wulf, N. Keijzer, E. de Graaff, M. Fukuda, I.T. Shepherd, A. Akhmanova, and C.C. Hoogenraad. 2010. Pericentrosomal targeting of Rab6 secretory vesicles by Bicaudal-D-related protein 1 (BICDR-1) regulates neuritogenesis. *EMBO J.* 29:1637–1651. https://doi.org/10.1038/emboj.2010.51

Schlager, M.A., H.T. Hoang, L. Urnavicius, S.L. Bullock, and A.P. Carter. 2014. In vitro reconstitution of a highly processive recombinant human dynein complex. *EMBO J.* 33:1855–1868. https://doi.org/10.15252/embj.201488792

Schroeder, C.M., and R.D. Vale. 2016. Assembly and activation of dynein-dynactin by the cargo adaptor protein Hook3. *J. Cell Biol.* 214:309–318. https://doi.org/10.1083/jcb.201604002

Schroeder, C.M., J.M. Ostrem, N.T. Hertz, and R.D. Vale. 2014. A Ras-like domain in the light intermediate chain bridges the dynein motor to a cargo-binding region. *eLife.* 3:e03351. https://doi.org/10.7554/eLife.03351

Scott-Solomon, E., and R. Kuruvilla. 2018. Mechanisms of neurotrophin trafficking via Trk receptors. *Mol. Cell. Neurosci.* 91:25–33. https://doi.org/10.1016/j.mcn.2018.03.013

Szebenyi, G., B. Hall, R. Yu, A.I. Hashim, and H. Krämer. 2007. Hook2 localizes to the centrosome, binds directly to centriolin/CEP110 and contributes to centrosomal function. *Traffic.* 8:32–46. https://doi.org/10.1111/j.1600-0854.2006.00511.x

Terawaki, S., A. Yoshikane, Y. Higuchi, and K. Wakamatsu. 2015. Structural basis for cargo binding and autoinhibition of Bicaudal-D1 by a parallel coiled-coil with homotypic registry. *Biochem. Biophys. Res. Commun.* 460:451–456. https://doi.org/10.1016/j.bbrc.2015.03.054

Urnavicius, L., K. Zhang, A.G. Diamant, C. Motz, M.A. Schlager, M. Yu, N.A. Patel, C.V. Robinson, and A.P. Carter. 2015. The structure of the dynactin complex and its interaction with dynein. *Science.* 347:1441–1446. https://doi.org/10.1126/science.aaa4080

Urnavicius, L., C.K. Lau, M.M. Elshenawy, E. Morales-Rios, C. Motz, A. Yildiz, and A.P. Carter. 2018. Cryo-EM shows how dynactin recruits two dyneins for faster movement. *Nature.* 554:202–206. https://doi.org/10.1038/nature25462

Watson, F.L., H.M. Heerssen, A. Bhattacharyya, L. Klesse, M.Z. Lin, and R.A. Segal. 2001. Neurotrophins use the Erk5 pathway to mediate a retrograde survival response. *Nat. Neurosci.* 4:981–988. https://doi.org/10.1038/nn720

Wu, M., T. Wang, E. Loh, W. Hong, and H. Song. 2005. Structural basis for recruitment of RILP by small GTPase Rab7. *EMBO J.* 24:1491–1501. https://doi.org/10.1038/sj.emboj.7600643

Xu, L., M.E. Sowa, J. Chen, X. Li, S.P. Gygi, and J.W. Harper. 2008. An FTS/Hook/p107(FHIP) complex interacts with and promotes endosomal clustering by the homotypic vacuolar protein sorting complex. *Mol. Biol. Cell.* 19:5059–5071. https://doi.org/10.1091/mbc.e08-05-0473

Yao, X., X. Wang, and X. Xiang. 2014. FHIP and FTS proteins are critical for dynein-mediated transport of early endosomes in Aspergillus. *Mol. Biol. Cell.* 25:2181–2189. https://doi.org/10.1091/mbc.e14-04-0873

Ye, H., R. Kuruvilla, L.S. Zweifel, and D.D. Ginty. 2003. Evidence in support of signaling endosome-based retrograde survival of sympathetic neurons. *Neuron.* 39:57–68. https://doi.org/10.1016/S0896-6273(03)00266-6

Ye, M., K.M. Lehigh, and D.D. Ginty. 2018. Multivesicular bodies mediate long-range retrograde NGF-TrkA signaling. *eLife.* 7:e33012. https://doi.org/10.7554/eLife.33012

Yeh, T.-Y., N.J. Quintyne, B.R. Scipioni, D.M. Eckley, and T.A. Schroer. 2012. Dynactin's pointed-end complex is a cargo-targeting module. *Mol. Biol. Cell.* 23:3827–3837. https://doi.org/10.1091/mbc.e12-07-0496

Zhang, J., X. Yao, L. Fischer, J.F. Abenza, M.A. Peñalva, and X. Xiang. 2011. The p25 subunit of the dynactin complex is required for dynein-early endosome interaction. *J. Cell Biol.* 193:1245–1255. https://doi.org/10.1083/jcb.201011022

Zhang, J., R. Qiu, H.N. Arst Jr., M.A. Peñalva, and X. Xiang. 2014. HookA is a novel dynein-early endosome linker critical for cargo movement in vivo. *J. Cell Biol.* 204:1009–1026. https://doi.org/10.1083/jcb.201308009

Zhang, K., H.E. Foster, A. Rondelet, S.E. Lacey, N. Bahi-Buisson, A.W. Bird, and A.P. Carter. 2017. Cryo-EM Reveals How Human Cytoplasmic Dynein Is Auto-inhibited and Activated. *Cell.* 169:1303–1314.e18. https://doi.org/10.1016/j.cell.2017.05.025

Zhou, B., Q. Cai, Y. Xie, and Z.-H. Sheng. 2012. Snapin recruits dynein to BDNF-TrkB signaling endosomes for retrograde axonal transport and is essential for dendrite growth of cortical neurons. *Cell Reports.* 2:42–51. https://doi.org/10.1016/j.celrep.2012.06.010